RSC Advances

ROYAL SOCIETY
OF CHEMISTRY

www.rsc.org/advances

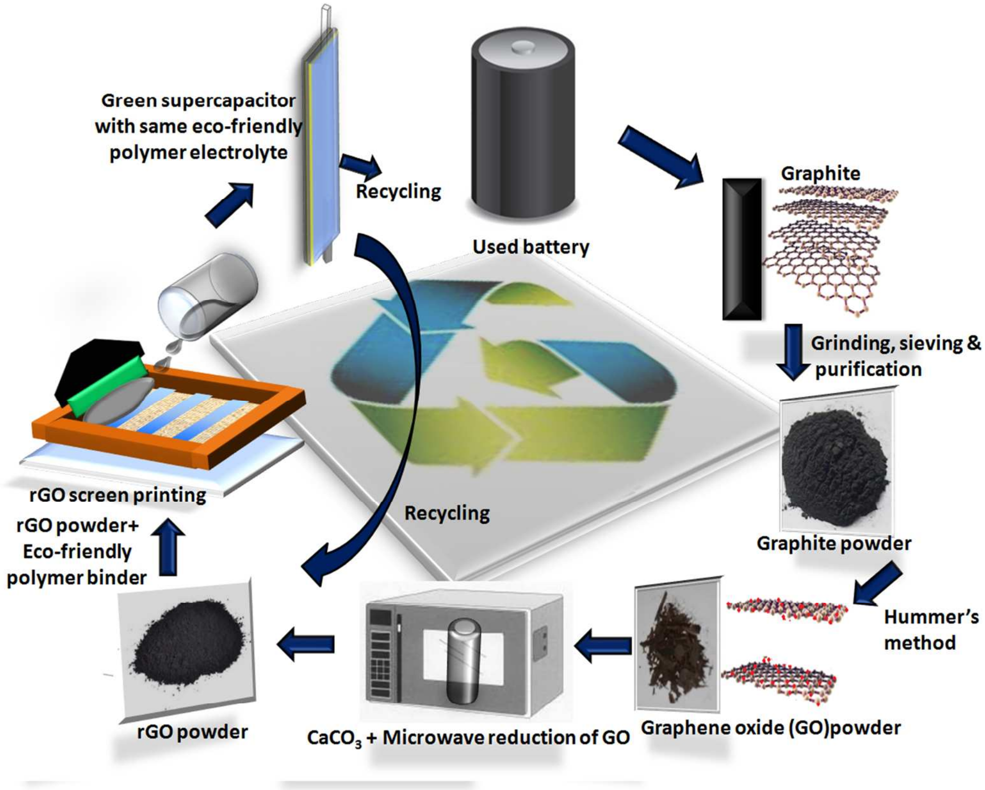

Schematic preparation and fabrication of eco-friendly supercapacitor

Reduced graphene oxide derived from used cell graphite, and its green fabrication as eco-friendly supercapacitor

Y. N. Sudhakar[1], M. Selvakumar[1*], D. Krishna Bhat[2], S. Senthilkumar[3]

[1]*Department of Chemistry, Manipal Institute of Technology, Manipal, Karnataka, India.*

[2]*Department of Chemistry, National Institute of Technology Karnataka, Surathkal, Mangalore, India.*

[3]*Department of Electrodics and Electrocatalysis, Central Electrochemical Research Institute, Karaikudy, Tamil Nadu.*

*Corresponding author: chemselva78@gmail.com

Graphite extracted from the used primary cell was converted into reduced graphene oxide (rGO) using calcium carbonate along with rapid and local joule heating of microwave irradiation. Electrodes were prepared by ultrasonically dispersing rGO in biodegradable poly(vinylpyrrolidone) (PVP) binder and coating on recyclable poly (ethyleneterephthalate) (PET) sheet using the low-cost screen printing technique. Utility of same polymer (PVP) as binder as well as solid polymer electrolyte (SPE) enhances the compatibility and ionic conductivity properties of the hydrophobic rGO electrode in the supercapacitor system. Further, the phosphoric acid (H_3PO_4) doped biodegradable SPE were screen printed for the first time on the rGO electrodes. Ionic conductivity and dielectric studies of the SPE were carried out at different temperatures and different dopant acid concentrations. The morphology, composition and structure of the graphene electrode components were characterized using Fourier transform infrared spectroscopy, Raman spectroscopy, X-ray diffraction, scanning electron microscopy and X-ray photoelectron spectroscopy methods. Transmission electron microscopy images showed single to few layer of rGO sheets and selected area electron diffraction exhibited presence of slight defects. The fabricated environment friendly, industrially favorable and green supercapacitor showed specific capacitance of 201 F g^{-1} and cyclic stability with 97% retention of the initial capacitance over 2000 cycles. Furthermore, the performance of this green supercapacitor is comparable to that of fabricated using rGO synthesized from commercial graphite and other reported literatures.

Key words: reduced graphene oxide, binder, biodegradable, supercapacitor

Introduction

The significance of an energy device like supercapacitors which provides a short load cycle for applications in memory back-up systems, electric vehicles, displays, and energy capture from solar cells has gained attention of many researchers in the last decades.[1] In this uprising of supercapacitor research many materials have been synthesised or modified for achieving the desired properties. Nevertheless, durability of energy devices lasts for 100 to millions discharge cycles and later they are dumped in the landfills. Since the ban of usage of mercury in the primary battery, they are considered to be less harmful to the environment, but many countries are implementing battery directives,[2] which insists the battery manufacturers to collect and recycle the used batteries for the safety of the near future. Primary batteries such as zinc-carbon, alkaline batteries and secondary rechargeable alkaline manganese batteries utilize graphite as the cathode material. Graphite is becoming an important raw material in many applications like energy devices, micro-sensors, super-adsorbents, semiconductors[3-6] etc. The fact that graphite has a wider range of both current and emerging uses; graphite's demand and disposal raise concern on the cost and environmental issues. With the increase in research and technologies for the betterment of these devices there will be a 100 times increase in the global graphite requirements than present demand. Although, presently graphite is available in abundance in nature, sooner or later, to meet the hyper demand of graphite, it will be considered similar to rare earth materials from key supplier countries for profitable business. This would impact global demand, price hike and need for purer graphite. Recycling industries will certainly get boosted and decrease the environment impact of battery disposals. A patent has also been filed for obtaining low cost graphite from recycled tyres for lithium batteries.[7] We are inspired by the statement that the ‘‘greenness’’ of a battery does not only depend on what kind of material is used in the battery, but also on how well the battery is managed throughout its life[8,9]. Hence, we extend an effort to join the ongoing green revolution to use the graphite from worn out primary cell as electrode material for supercapacitors. Usually, the high purity graphite is used as cathode material in primary cell like zinc-carbon cell.[10] When compared to commercial graphite, cell graphite is highly crystalline and contains traces of carbon black. This requires a simple process to bring about amorphous character and extract pure graphite, and finally convert it into rGO.

For conversion of graphite to rGO many methods have been used.[11,12] Few green methods have also been implemented like the one by Chen,[13] without the use of polymer or surfactant. But, the use of ammonia in this method is a concern when considered in large amounts. Microwave treatment has also been used for exfoliation of graphite oxide to rGO.[14]

The green method wherein ionic liquid assisted microwave reduction of GO gave a specific capacitance of 135 F g^{-1} and was reported to be rapid and facile.[15] Using Gum Arabic and ultrasonification graphite was exfoliated, but again the concern is that to bring about 100% pure graphene, 100 hrs of ultrasonification and acid treatment was required.[16] Similarly, many attempts have been made to develop eco-friendly methods to prepare rGO,[17-22] which is usually associated with complex processes for removal of reducing agents. Using sodium carbonate, rGO was efficiently reduced from GO but yet took 4 hr for reduction.[23] Hence, in this study, a new approach of microwave treatment was employed along with environmentally abundant calcium carbonate to produce rGO from graphene oxide solution efficiently within few minutes.

Graphene has been used as electrode material in supercapacitors.[1,24-26] A single atomic layer of graphene having high surface area is idealistic electrode material, but removal of heteroatoms and functional groups completely will affect the capacitance.[27] Graphene is known to have a theoretical surface area of 2630 m^2 g^{-1} and Hantel et al.[28] claimed to have achieved 2687 m^2 g^{-1} from partially reduced graphene oxide. Fewer layers of graphene showed 1400 m^2 g^{-1} surface area[29] and porous as prepared using microwave.[30] Highly porous 3D graphene produced from biomass showed good conductivity and specific capacitance of 231 F g^{-1}.[31] Graphene and rGO are slight different in structure, since rGO has more lattice defects and trace amount of functional groups when compared to graphene. The rGO/polymer binder having mesoporous rGO was reported for good ionic liquid accessibility and hence showed specific capacitance of 250 F g^{-1}.[32] Even macroporus low BET surface area significantly adsorbed oil better than micro or mesoporous graphene sheets.[5] Nonetheless, compared to surface area of carbon nanofibers and activated carbon, rGO has a lower surface area, but still some of these unique properties make rGO use as electrode material for supercapacitors especially in acid doped electrolytes. The surface hydrophobicity and poor dispersibility[33] property of graphene makes the accessibility of liquid electrolytes difficult to form a double layer at electrode/electrolyte interface region. Hence, in this study an eco-friendly biodegradable PVP was used as a binder. PVP has great wetting property since it stays sticky even at high humidity conditions and it is normally used as a binder in printing technology.

Lithium ion energy devices are considered to be having high energy density and widely used even though it is still associated with the risk of safety accidents because of the flammability of the organic electrolytes. The use of same polymer as electrolyte as well as separator has been demonstrated for much safer, lighter and flexible energy devices.[34,35]

Nevertheless, environmental factors must be considered since polymer electrolytes so far used are obtained from petroleum sources and separators used cannot be recycled.[36,37] In concern to the environment, as per our knowledge we had first prepared solid biodegradable polymer electrolytes for use in supercapacitor.[38] Although, the use of lithium salts in these electrolytes showed good specific energy, they are still harmful when used in large amounts. Even though lithium salts are available in abundance, the large requirements of energy devices like batteries makes the cost and dependability on supply to increase, and more concern to the environment since lithium cannot be yet recycled with high purity. Therefore, phosphoric acid was used as a dopant in the present system. Many stable polymer electrolytes based on H_3PO_4, H_2SO_4 and other strong acids have been reported to have conductivity ranging from 10^{-2}-10^{-5} S cm^{-1}.[39-41] Since conductivity depends on the acid and water concentration,[42] the polymer used must be in favour of proton conduction and have good water retention property. The solid polymer electrolytes (SPEs) were adapted to thick film having desired viscosity and adhesive property suitable for screen printing.

Printing techniques are manufacturing friendly and uniformity of coating is high, thereby one can achieve the desired output easily from the coated material. Although, a good coating of graphene with better property was achieved by transfer printing process[43] it still requires special tuning for adhesion to substrate. Inkjet printed rGO electrode showed a low voltage window in cyclic voltammetry.[44] Roll coating, spin coating and screen printing are shown to have useful in many electrodes, sensors and OLEDs.[28,45-47] Compared to roll and spin coating methods, screen printing can be done in large scale with uniform thickness and within a short period of time. Screen printing inks are also beneficial since dry matter content of the ink can be extremely high.[48] Lu et al. observed that the surface area of the rGO was not harmed by a screen printing method.[46] Recently, screen printed rGO/polyaniline electrodes achieved specific capacitance of 236 F g^{-1}.[49] Hence, this eco-friendly and low cost screen printing method was used for coating rGO on PET substrate. To avoid the leakage due to liquid electrolyte and complex packing of the supercapacitor, we use phosphoric acid (H_3PO_4) doped biodegradable PVP as solid polymer electrolyte (SPE). The basic idea is to bring about good adhesion of the PVP electrolyte with the rGO/PVP binder electrode and thus enhance the double layer formation between the electrode/electrolyte interface.

In view of the aforementioned aspects, we report here for the first time a complete environmental friendly green supercapacitor fabricated using rGO derived from used cell graphite as an electrode material along with biodegradable PVP binder and H_3PO_4 doped PVP as a SPE. The characterizations of the prepared graphene-like material and PVP were done using Fourier transform infrared spectroscopy (FTIR), Raman spectroscopy, X-ray diffraction (XRD), scanning electron microscopy (SEM) and X-ray photoelectron spectroscopy (XPS), Transmission electron microscopy (TEM), selected area electron diffraction (SAED) methods and electrochemical techniques. Differential scanning calorimetry and biodegradation studies can be found in Fig S1 (S: Supplementary Figure) and Fig S4 of supplementary information. Ionic conductivity and dielectric studies of the SPE (PVP/H_3PO_4, different concentration ratios) were carried at different temperature and respective activation energy was calculated. Screen printed silver paste was used as a current collector. The supercapacitor properties like cyclic voltammetry (CV), AC impedance and galvanostatic charge/discharge (GCD) studies were determined. The results have also been simultaneously compared with supercapacitor fabricated using rGO derived from commercial graphite.

Experimental

Materials

Completely discharged AA or AAA size zinc-carbon primary cells of various companies were collected from the nearby collecting shop. PVP K30 (LobaChemi) for binder and PVP (Mol. Wt. 40,000, LobaChemi) for solid electrolyte were used as obtained. H_3PO_4 (85%, Merck) was used as dopant acid. Screen printable silver ink was purchased from Toyo ink (Japan). Print grade A-PET sheet was used for study.

Conductivity measurements

Blocking emery polished stainless steel (SS) sheets were taken as current collectors for the ionic conductivity measurements. SPEs were prepared by mixing PVP (high molecular weight) and 1.0 M H_3PO_4 in 2:0.5, 2:1, 2:1.5 and 2:2 wt% ratios, respectively. Calculated amount of Millipore water was added drop wise to these mixtures until a jelly texture is developed. Required amounts of prepared jelly inks were screen printed 2 times on the separate SS sheets. The ink dispersed slowly and occupied mesh marks during drying in vacuum oven at 60 °C for 2 hr. The thickness of SPEs was ~0.1 mm. The screen printed SS sheets were cut into 3×2 cm electrodes and fastened using adhesive on another SS electrode by simple hand pressure. The ionic conductivity of the SPE was measured in a cell by a complex impedance method in a frequency range of 1 MHz to 100 mHz using a small amplitude AC signal of 10 mV. The ionic conductivity of the SPE was calculated from the measured bulk resistance, area and thickness of the polymer thin film, by using the equation: $\sigma = L/R_bA$, where L is the thickness of the polymer electrolyte (cm), A is the area of the blocking electrode (cm^2), and R_b is the bulk resistance of the polymer electrolyte. From these AC impedance data, dielectric studies were carried out. The formulae and relationships between complex impedance, dielectric permittivity and dielectric modulus can be found elsewhere.[50] PVP is hygroscopic in nature; the influence of ambient humidity must be taken into account while studying at different temperatures. The ambient humidity in the cell was thus equilibrated with the water content in the SPE during the measurements. The temperature dependence on the ionic conductivity was measured by using a PID controlled oven (SES instruments, model PID 200) under a controlled temperature range of 20–80 °C by giving sufficient time interval at each temperature to secure the sample being in equilibrium.

Preparation of rGO from battery graphite

The used primary cells were cut open and the graphite rod was carefully removed. The rods were washed with Millipore water and subjected to polishing using emery paper. Rods were crushed using pestle mortar and washed with Millipore water to ensure removal of impurities of primary cell material. Lustrous powder was obtained after drying. The graphite powder was sieved using 100 micron mesh. Graphite powder was oxidised to graphite oxide using modified Hummers method.[51,52] Graphite oxide obtained was washed several times with Millipore water until the suspension attained a pH of 7. Further, suspension was subjected to ultrasonification for 30 min to obtain brownish graphene oxide (GO) solution. Centrifugation was carried out at 2000 rpm for 20 min and dried in vacuum oven to get GO flakes. $CaCO_3$ was mixed with GO flakes in 1:2 wt% ratios and suspended in 20 ml Millipore water. The solution mixture was kept in domestic microwave oven and exposed to medium microwave for 10 min. Typically, obtained hydrophobic rGO suspension associated with calcium salts was removed by adding 1M HCl and washed several times with Millipore water. Little amount of the obtained slurry was flame tested to ensure absence of brick red color due to calcium ions in the suspension. The slurry was dried in a vacuum oven for 2 hr at 60 °C.

Electrode preparation and fabrication of supercapacitors

The dried rGO powder was mixed well with PVP binder at 4:1 ratio. Calculated amount of Millipore water was added drop wise to the mixture until a paste is obtained (~1 g ml^{-1}). The paste was ultrasonicated for 10 min and allowed to set at ambient temperature for 2 hr. Using 200 micron mesh and manual screen printing technique, the rGO/PVP paste was coated on to PET surface. The coated materials were dried in vacuum oven at 60 °C for 2 hr.

Conductive silver ink was screen printed using 100 micron mesh on the edges of the rGO/PVP binder coated area and allowed to dry at ambient temperature. The weight of electrode material were ~3 mg. Electrical conductivity of the electrodes was studied using four-point probe method (SES instruments, Roorkee).

A PVP/ H_3PO_4 polymer electrolyte solution exhibiting a high ionic conductivity was screen printed 2 times on the prepared rGO electrode and allowed to set at 50 °C for 1 hr. Supercapacitor was fabricated as follows; the prepared rGO electrode containing SPE was cut into a 3 cm × 2 cm piece and placed on another rGO electrode without SPE and fastened using non-conducting adhesive by simple hand pressure.

Characterization

FTIR measurements of the graphite, graphene oxide (GO), rGO, rGO/PVP binder, un-doped and acid doped PVP polymer electrolyte were carried out at room temperature using Shimadzu FTIR 8400S (Japan) spectrophotometer. KBr disk method was employed for this study. The micro SEM images were taken using ZEISS EVO 18 Special Edition. TEM and SAED images were obtained from Tecnai 20 G2, (Netherland). XRD was studied using Rigaku's MiniFlex 600. XPS was determined using non-monochromatic Al Kα X-ray source (1486.6 eV) with pass energy of 50.0 eV for the general scan and 40 eV for the core level spectra of each element. Laser-Raman was analyzed using Renishaw Invia Raman Microscope having source: He-Ne Laser 633 nm, 18 mW. DSC measurements were taken on first run using Shimadzu DSC 60 model instrument under nitrogen atmosphere (Fig. S1). Electrochemical characterization was carried out by CV, AC impedance and GCD studies. All the electrochemical studies were carried out using a BioLogic SP-150 instrument.

Results and discussion

Possible reduction mechanism of GO

$CaCO_3$ was used for reducing GO. $CaCO_3$ in aqueous medium produces calcium and carbonate ions. Furthermore, carbonate ions undergo hydrolysis gives hydroxide ions and bicarbonate ions, which again hydrolysis to produce hydroxide ions.[23] These hydroxide ions show high polarizability and efficiently absorb microwave energy and generate heat which in turn reduces the GO within few min. Moreover, GO undergoes strong deoxygenation in strong alkali solutions.[53,54] The $CaCO_3$-rGO mixture can be separated by adding dilute HCl followed by several centrifugations. The role of $CaCO_3$ is not only as reducing agent but it is also useful to remove the un-reacted H_2SO_4 used during Hummer's method, this $CaCO_3$ will readily react to form $CaSO_4$, CO_2 and water. Thus, extensive cleaning after oxidation of graphite can be easily managed.

Conductivity and dielectric studies

The ionic conductivities of the SPEs calculated at different temperatures using R_b values taken from AC impedance spectra are shown in Fig. 1a. The ionic conductivities increased with increase in acid concentration and temperature. The temperature dependence of the conductivity follows Arrhenius equation $\sigma = \sigma_o \exp(-E_a/k_oT)$, where E_a is activation energy for conduction, σ_o is the pre-exponential factor and k_o is the Boltzmann constant. It implies that, for higher acid concentration, ionic conductivity occurs by means of vehicle type mechanisms in the SPE matrix. While, lower concentration of acid proton transfer takes place via interstitial water pathway i.e., Grotthus type mechanism.[55] This is confirmed by E_a values as a function of acid concentration i.e., ranging from 0.11-0.30 eV. The Nyquist plot of sample with highest ionic conductivity is shown in Fig. 1b since similar pattern of spectra were obtained for all the SPEs under investigation. The highest ionic conductivity value of 2.2×10^{-4} S cm^{-1} was reached at 80 °C. Depressed semicircular arc at higher frequency region was observed due to the migration of protons through polymer electrolyte. In contrast, at low frequency region a spike was observed to be angled towards real part of impedance spectra which is attributed to the double layer/polarization at the electrode/electrolyte interface and associated hindrance to diffusion of ions towards electrode. Considering the effect of temperature on the SPEs, the R_b value decreased due to the enhancement in the segmental motion of the polymer chains revealing viscous channels (hydrogen bonded water) for proton mobility.

Fig. 2a depicts dielectric constant (ε_R) as a function of frequency wherein ε_R decreases with increasing frequency. Since protons are unable to exchange with the blocking electrodes a non-Debye type behavior was observed at low frequency region. Whilst, in high frequency region high periodic reversal of the electric field occurs at interface reducing the contribution of charge carriers towards the electrode. The variation of dielectric constant would be due to hopping conduction mechanism similar to dielectric polarization.[56] High dielectric constant indicates well dissociation of acid in the polymer system. Also, as the temperature increases the dielectric constant increases due to increase in orientation of dipoles in the direction of the applied field and hence, increasing the ionic conductivity of the SPE. Fig. 2b depicts dielectric loss (ε_I) as a function of frequency wherein ε_I decreases with increasing frequency. In acid based SPE, the role of water in the ionic conductivity is important since free charge carriers significantly affect the polarization at the electrode/electrolyte interface. It was observed that ε_I increases at low frequency and decreases at higher frequency region. It is worth noting that there is no relaxation peaks due to charges building up at the interface during the free charge motion within the material. The ε_I increased with increase in the temperature indicating that water largely influences the ionic conductivity in the sample. Fig 2c and d shows real, M_R and imaginary, M_I, parts of electrical modulus as a function of frequency. Electric modulus study helps to understand the frequency influence on the bulk of the SPE since polarization is negligible in this analysis. M_R shows a long tail feature at low frequency region indicating capacitive nature of the SPE.[57] With increase in temperature less variation was observed due to the fast motion of the proton in the bulk and confirmed in AC impedance studies. M_I show peaks at higher frequency region which can be attributed to ionic conduction of protons which are spatially confined to their potential wells and perform only localized motion. As the temperature increased, the M_I decreased liberating these ionic wells and thereby confirming the Grotthus-type mechanism in which a proton moves rapidly from H_3O^+ to a hydrogen bonded water molecule and is transferred further along a series of hydrogen-bonded water molecules by a rearrangement of hydrogen bonds.[58]

Characterization

The structure and distribution properties of cell graphite, rGO+binder, and rGO were characterized using XRD analysis, as shown in Fig 3a. For battery graphite, the intensive and sharp peaks at 2θ=25.8° and 2θ=22.5° indicated the highly organized layered structure with interlayer spacing of 0.34 to 0.39 nm, respectively.[59] Lattice defects were observed due to breakdown of hexagonal symmetry of graphite induced by mechanical grinding.[60] After reduction the low intensity peaks were observed and was found to be shifted to 2θ=15.0° and 2θ=22.1°, corresponding increase in interlayer spacing of 0.58 nm and 0.41 nm. This indicates efficient exfoliation of battery graphite during microwave reduction of GO in presence of $CaCO_3$. A broad peak observed after mixing of PVP binder with rGO shows uniform distribution of rGO in the polymer matrix and yet maintaining rigid structure enough for easy access to ions during charging and discharging. Although the high peak was observed at 2θ=21.4°, the interlayer spacing was 0.41 nm which was found to be same as the rGO. This implies that the binder was able to decrease the crystallinity of rGO to some extent but could not penetrate between the two graphene sheets. When compared with XRD pattern of commercial graphite (Fig. S2a), the intensity of battery graphite was much higher indicating high crystallinity nature. rGO obtained from commercial graphite showed broad peaks than rGO from battery graphite indicating that our reduction process was able to bring amorphous characteristics of rGO sheets having few layers.

Raman spectroscopy was used as a nondestructive tool to characterize structural changes like disorders and defects. D and G band are expected in the Raman spectra of graphite and rGO which are correlated to first order scattering of E_{2g} phonons of sp^2-bonded carbon atoms and *j*-photons of A_{1g} symmetry of sp^3-bonded carbon atoms of disordered rGO.[61] As shown in Fig. 3b, for GO the D band appeared at 1384 cm^{-1} and G band locates at 1627 cm^{-1}, while for rGO the D band shifted and broadened at 1346 cm^{-1} and G band 1598 cm^{-1} indicating reduction of GO[59] during microwave treatment. The peaks at ~2700 cm^{-1} referred as 2D peaks since it is second order of D peak also behaves similarly in shifts with respect to GO and rGO. Furthermore, a significant change in shape and intensity of the 2D peak of rGO are observed compared to GO and roughly five times more intense than G peak. This results matches with the reference[62] and gives indication of varying few number of layers in rGO.

Fig. 3c shows FTIR spectra of battery graphite, GO and rGO. Graphite spectrum showed skeletal vibrations at 1600 cm^{-1}, while no other significant peak was found. In GO the presence of different type of oxygen functionalities was confirmed at 3401 cm^{-1} due OH stretching vibrations. Stretching vibrations due to C=O, C-OH and C-O at 1720 cm^{-1}, 1220 cm^{-1} and 1060 cm^{-1}, respectively.[63] The intensity of peak at 1620 cm^{-1} was increased suggesting the increased adsorbed water molecules. After reduction of GO the OH stretching at 3401 cm^{-1} significantly reduced, while trace quantity of C=O at 1720 cm^{-1} still remained along with C-O at 1060 cm^{-1}. However, the phenol C=C ring stretching at 1587 cm^{-1} were observed.[64] The absence of CO_3^{2-} group which forms weak peak at 870 cm^{-1} and intensive peaks at 1465 and 1530 cm^{-1} indicates complete removal of carbonate impurities associated with rGO during the reduction process. Fig. 3d shows FTIR spectra of pure PVP and H_3PO_4 doped PVP SPE. The C=O stretching band at 1670 cm^{-1} for pure PVP sharpened in addition of acid indicating strong interactions. The asymmetric stretching at 2954 cm^{-1} and symmetric stretching at 2890 cm^{-1} (CH_2) were less intensive. Less intensive –C–N stretching vibrations and –C–H bending vibrations of the acid doped PVP polymer were observed at 1285 and 1443 cm^{-1}, respectively when compared to pure PVP. This indicates the acid is well dissociated in the PVP matrix leading to interactions with the polymer chains. Typical PO_4^{3-} group formed intensive peaks at 570-600 cm^{-1} and at 1100 to 1200 cm^{-1}.[65] The peaks at 3480 cm^{-1} were relatively due to adsorbed water in both the samples. The spectrum of PVP binder+rGO shows similar characteristics of acid doped PVP the only difference was absence of PO_4^{3-} group. This also implies that a non-covalent interaction exists between rGO and PVP binder which would play an important role in stability of the electrode material, while maintaining the spongy nature for easy accessibility of ions. FTIR spectra (Fig. S2b) of commercial derived graphite materials showed similar characteristic peaks of battery graphite, but upon reduction the rGO spectrum showed very low intensity of OH, C=O and C-O. This result of commercial rGO is confirming the XRD results implying complete reduction of GO using $CaCO_3$ and microwave heating.

Fig. 4a shows C1s XPS spectrum of GO after deconvolution. The peaks specifies a considerable degree of oxidation of graphite corresponding to carbon atoms in different functional groups, which is observed at 284.2, 284.8, 286.1, and 288.4 eV originating from C-C, C-O, C=O, and O-C=O groups, respectively. In Fig. 4b the O1s XPS spectrum of GO shows peaks at 529.4 and 532 eV from C=O and C-O, respectively. However, after microwave treatment the peaks of rGO (Fig. 4c and d) reduced slightly and shifted to higher binding energy region. The peaks at 286.9, 287.4, 288.7 and 290.2 corresponding to C-C, C-O, C=O and O-C=O, decreased significantly indicating efficient deoxygenation of GO and the formation of rGO.[59] Furthermore, the calculated C/O ratio changed from 1.75 to 4.40. Nevertheless, the intensity in O1s spectrum of rGO remained the same but slightly shifted to higher binding energy and sharpened. This implies trace amount of C-O groups are associated with the rGO.

Fig. S3 representing SEM image of battery graphite powder show hexagonal rods along with defects due to crushed graphite grains having size ranging from 2-4 μm. Fig. 5a illustrates the SEM image showing particle size of rGO powder ranging from 500 to 800 nm obtained by $CaCO_3$ and microwave treatment of GO. Almost regular grain size broken from the hexagonal rod structure of graphite with agglomeration having mesoporus structures was obtained. The Fig. 5b (front view) and c (cross section view) shows SEM images of screen printed rGO and PVP binder. The images suggest that rGO particles are less aggregated with few clumped sheets and are stuffed in PVP binder. This PVP prevents rGO from re-stacking during pressure applied for fabrication of supercapacitor. Due to this morphology, the ions can readily access not only 2D structure of rGO but also 3D structure wherein well wetted PVP chains provides channels for the ions for easy access through these stuffed rGO grains, hence, contributing to capacitance.

Fig. 6a depicts the TEM images of graphene sheets ranging from single to few layers which is found to be similar to rGO reported by Stoller et al.[66] Rippling structure, folding and scrolling nature of the rGO sheets are observed. Agglomerations are also observed illustrating how both sides of the graphene sheets are difficult to be accessed by the electrolyte. Therefore, the use of same polymer as binder and SPE creates passage of ions between these graphene sheets. However, the layer counting was not confirmed by TEM and even uncertain number of layers was evident from Raman spectra. In Fig. 6b, the selected area electron diffraction (SAED) showed multiple hexagonal rings of different intensity and spot size on the same circle confirming the random orientation of graphene layer within graphene sheets.[67] The existence of few sheets and occurrence of spots in different positions other than circle having hexagonal pattern shows the presence of oxygen and hydroxyl groups in few graphene sheets, but it is worth mentioning that almost all oxygen and hydroxyl groups are expelled using rapid, facile microwave treatment in presence of $CaCO_3$.

The eco-friendly aspects of SPEs were measure using soil burial biodegradation method (Fig. S4). The SPEs having different acid concentrations showed higher degradation indicating higher concentration of acid is able to break the intermolecular bonding of polymer chains and created more sight for degradation.

Supercapacitors studies

Fig. 7a shows the CV of fabricated supercapacitor as a function of scan rates. All the curves were nearly rectangular, which is characteristic of ideal capacitor. As the scan rate increased there was less distortion in the curves and high rate properties. This suggests that there exists a high charge transfer kinetic at the electrode-electrolyte interface. The specific capacitance values of the supercapacitors have been calculated using the equation;[68]

$$C_s = \frac{2I}{\Delta V \times m} \tag{1}$$

where I is the average current, ΔV is the potential window, v is the scan rate and m is the mass of materials at each electrode. The factor of 2 is used because the series capacitance is formed in a two-electrode system. The maximum specific capacitance value is 201 F g^{-1} at 2 mV s^{-1}. The specific capacitance value is almost similar to the value of specific capacitance obtained from rGO prepared from commercial graphite (Fig. S5). Although the battery graphite was more crystalline than commercial graphite, the reduction of GO using $CaCO_3$ and microwave was able to bring uniform grains size of rGO, thus obtaining similar specific capacitance. Hence, the rGO obtained from used battery graphite can be effectively used as electrode material.

Normally, electrochemical double layer are formed between electrode and electrolyte, rather than storing in bulk of the SPE. Nyquist plot (Fig. 7b) of green supercapacitor typically helps to understand the importance of using same polymer as binder and SPE. A small semicircle arc at high frequency region, which represents the intrinsic internal resistance of electrode material and electrolyte, followed by almost 45° Warburg impedance in low frequency region, which is the trend of ideal capacitive behaviour, and agrees to CV results. Small semicircle at high frequency region implies low intrinsic internal resistance due to improved hydrophilicity of the rGO material/PVP electrode materials, resulting to enhance wettability and facilitated rapid electrolyte ion transport within the spacing of graphene layers and polymer chains.[69] In addition the ionic diffusion at middle frequency region is achieved very fast, and a more vertical line at low frequency region, indicating the supercapacitor has higher ionic conductivity and electrochemical performance.[70] Thus, introducing surface PVP as binder to rGO along with same PVP based SPE appears to be an effective way of improving an electrode's capacitance. Similar pattern was observed for rGO derived from commercial graphite, but with less resistivity value (Fig. S5). The values of fitted circuit R1+Q2/(R2+W2) can be found in Table S1.

Fig. 7c shows normalized imaginary part (reactive power) $|Q|/|S|\%$ and real part (active power) $|P|/|S|\%$ of the complex power versus frequency plot of the supercapacitor at 303K. As observed the normalized imaginary part of power $|Q|/|S|\%$ increases as frequency decreases and maximum was reached, wherein the supercapacitor behaves like a pure capacitance. At the same time, when $|P|/|S|\%$ is 100% at high frequencies, the supercapacitor behaves like a pure resistance i.e., power is dispersed into the system and then $|P|/|S|\%$ decreases as frequency increases. The crossing of two plots appears when $|P|=|Q|$, referring to the time constant τ_0. The theoretical details of this plotting technique can be found elsewhere.[71] The calculated time constant was found to be equal to 3 ms and hence, indicates that the present system can be efficiently used at low frequencies.

In GCD studies, the curves with triangular symmetrical distribution indicate good capacitive properties of supercapacitor. Fig. 7d show the GCD curves of the supercapacitor at various current densities of 0.2Ag^{-1}, 0.4 Ag^{-1} and 0.6 A g^{-1}. The specific capacitance was derived from the charge–discharge curve according to the following equation[72]

$$C_s = \frac{I \times \Delta t}{\Delta V \times m} \tag{2}$$

where I is the applied discharge current, Δt is the discharged time after IR drop, ΔV is the discharge potential window after IR drop, and m is the mass of the single electrode materials, respectively. C_s values decreased with increasing current density 208, 184 and 162 F g^{-1}. Comparatively, the specific capacitance was almost same as 3D graphene based bulk materials[31] i.e., 231 F g^{-1} and even that of hydrazine reduced GO.[26] Fig. 7d results shows slight voltage drop due to ohmic resistance and quite good stability was exhibited at low current density. This implies that if the graphene layers with the binder chains are adjusted to the size of ions, the pore volume may become saturated by electrolyte species, limiting the maximum operating voltage and the energy stored in the supercapacitor.[73] Even the presence of hygroscopic PVP would largely interfere by promoting proton transfer within the spacing of rGO materials, thereby causing little deviation from ideal capacitor behaviour. However, with increase in current density the voltage drop decreased indicating sufficient amount of ions were accommodated and during discharge intercalation/insertion and trapping of ions were not observed. Therefore, supercapacitor performance was optimized with respect to wettability based on texture/structure of electrode material and SPE to a certain extent. A further hard core research is indeed required to understand the exact performance based on texture of carbon materials and optimized ionic conductors, rather than just concluding based on maximum capacitance.[64,74] The energy (E) and power (P) densities and equivalent series resistance (ESR) were calculated from the following equations,

$$E = \frac{C \times \Delta V^2}{2} \times \frac{1000}{3600} \tag{3}$$

$$P = \frac{I \times \Delta V}{2 \times m} \times 1000 \tag{4}$$

$$ESR = \frac{iR_{drop}}{2 \times I} \tag{5}$$

The maximum of E of 11 Wh kg^{-1} (with P of 2 kW kg^{-1}) at 0.2 A $g^{-1}$and P of 5 kW kg^{-1} (with E of 8 Wh kg^{-1}) at 0.6 Ag^{-1} was obtained. ESR value was 4.7 ohm. The E is found to be lower than that of other reported supercapacitors. Nevertheless, high value of the P is well suited for surge-power delivery applications.[75] Table 1 and 2 shows the comparison of specific capacitance, energy density and power density of supercapacitors having different electrode material prepared using various methods.

Cyclic durability is important electrochemical performances of supercapacitor for its practical application. The C_s variation at 0.2 Ag^{-1} with the cyclic times is shown in Fig. 7e. The specific capacitance was reversibly maintained with 97% retention of the initial capacitance over 2000 cycles. This superior performance was attributed to the excellent mechanical robustness, and intimate interfacial contact among the multiple components.[38] Since initial decrease of capacitance was less the use of same polymer as binder and SPE has minor effect when compared to other internal resistance in the device. Thus, this supercapacitor possesses good stability and a very high degree of reversibility in the repetitive charge-discharge cycling.

Scheme 1 shows preparation of supercapacitor by screen printing method and the possible mechanism of ion transport in the supercapacitor. Considering that the PVP has a strong water adsorption capability,[89] the dried rGO/PVP coating creates affinity for water. When SPE containing acid aqueous electrolyte was coated on the surface, the tendency of the electrode material for water absorption, readily accommodates some amount of the acid electrolyte and immediately creates channels for ionic movement by forming interactions with polymer chains of PVP and rGO layers. The addition of PVP binder avoids agglomeration of rGO which normally blocks the accessible surface of the rGO. At the point of contact of SPE and electrode material, a high degree of continuous and interconnected ionic transport channels would be formed. This forms a kind of adaptive rGO/PVP gel film for easy accessibility of ions. As discussed earlier the transport of protons takes place via Grotthus type in the SPE and easily gets transferred to electrode/electrolyte interface region, thereby forming double layer very rapidly. Thus, charging/discharging results in higher power density and stability.

Conclusion

In summary, we have successfully demonstrated the extraction of graphite from used cell and it's conversion to rGO using green microwave reduction method in the presence of $CaCO_3$ for the first time. This rGO was mixed with eco-friendly PVP binder and screen printed on PET substrate and supercapacitors was fabricated using these novel rGO electrodes and SPE. Such fabricated supercapacitor showed specific capacitance of 201 F g^{-1} at 2 mV s^{-1}. Ionic conductivity of the SPE was not significantly affected by the variation of temperature. The dielectric studies showed good capacitive behavior of the material and influence of water in the transport of protons. The characterization studies showed good interaction among rGO, PVP and SPE. High power density was exhibited with low ESR value. The high performance of the supercapacitor is attributed to the enhanced interaction between the adaptive electrode material and SPE. The obtained specific capacitance was comparable to that of the supercapacitor fabricated using rGO derived from commercial graphite.

Acknowledgment

The authors acknowledge with thanks the financial support received from the Defence and Research Development Organization (DRDO), Govt. of India, New Delhi. The facilities provided for printing by Manipal Technologies Limited, Manipal is greatly acknowledged.

Reference

1 L. L. Zhang, R. Zhou and X. S. Zhao, *J. Mater. Chem*., 2010, **20**, 5983.

2 http://pt.farnell.com/images/en_UK/rohs/pdf/battery_directive_nov08.pdf accessed July 2014.

3 F. Zhang, T. Zhang, X. Yang, L. Zhang, K. Leng, Y. Huang, and Y. Chen, *Energy Environ. Sci.*, 2013, **6**, 1623.

4 L. Huang, Y. Huang, J. Liang, X. Wan, and Y. Chen, *Nano Res.*, 2011, **4**, 675.

5 S. J. Yang, J. H. Kang, H. Jung, T. Kim, and C. R. Park, *J. Mater. Chem. A*, 2013, **1**, 9427.

6 L. Yan, Y. B. Zheng, F. Zhao, S. Li, X. Gao, B. Xu, P. S. Weiss, and Y. Zhao, *Chem. Soc. Rev.*, 2012, **41**, 97.

7 A. G. DeTrana, US Patent Application Filed: UTB 2980.0 "Pyrolytic Carbon Black Composite and Method of Making Same" Ref: 6321-434 [19079.0380]

8 R. Lankey and F. McMichael, Rechargeable Battery Management and Recycling: A Green Design Educational Module, Green Design Initiative Technical Report, Carnegie Mellon University, 1999, http://www.ce.cmu.edu/GreenDesign/gd/education/Battery.pdf, accessed July 2014.

9 P. Poizot and F. Dolhem, *Energy Environ. Sci.*, 2011, **4**, 2003.

10 http://www.baystreet.ca/articles/research_reports/fundamental_research/FMS-Update-Nov2012.pdf accessed July 2014.

11 S. Eigler, M. Enzelberger-Heim, S. Grimm, P. Hofmann, W. Kroener, A. Geworski, C. Dotzer, M. Röckert, J. Xiao, C. Papp, O. Lytken, H.-P. Steinrück, P. Müller, and A. Hirsch, *Adv. Mater.*, 2013, **25**, 3583.

12 L. Tang, Y. Wang, Y. Li, H. Feng, J. Lu, and J. Li, *Adv. Funct. Mater.*, 2009, **19**, 2782.

13 H. Chen, M. B. Müller, K. J. Gilmore, G. G. Wallace, and D. Li, *Adv. Mater.*, 2008, **20**, 3557–3561.

14 M. Cai, D. Thorpe, D. H. Adamson, and H. C. Schniepp, *J. Mater. Chem.*, 2012, **22**, 24992.

15 T. Kim, H. Chang Kang, T. Thanh Tung, J. Don Lee, H. Kim, W. Seok Yang, H. Gyu Yoon, and K. S. Suh, *RSC Adv.*, 2012, **2**, 8808.

16 V. Chabot, B. Kim, B. Sloper, C. Tzoganakis, and A. Yu, *Sci. Rep.*, 2013, **3**, 1378.

17 L. J. Cote, R. Cruz-Silva, and J. Huang, *J. Am. Chem. Soc*., 2009, **131**,11027.

18 G. Williams, B. Seger, and P.V. Kamat, *ACS Nano,* 2008, **2**, 1487.

19 Y. Wang, Z. Shi, and J. Yin, *ACS Appl. Mater. Int*., 2011, **3**, 1127.

20 K. H. Chang, Y. F. Lee, C. C. Hu, C. I. Chang, C. L. Liu, and Y. L. Yang, *Chem. Commun*., 2010, **46**, 7957.

21 W. Chen, L. Yan, and P. Bangal, *J. Phys. Chem. C*, 2010, **114**, 19885.

22 D. Zhang, X. Zhang, Y. Chen, C. Wang, and Y. Ma, *Electrochim. Acta*, 2012, **69**, 364.

23 Y. Jin, S. Huang, M. Zhang, M. Jia, and D. Hu, *Appl. Surf. Sci.*, 2013, **268**, 541.

24 Y. Sun, Q. Wu, and G. Shi, *Energy Environ. Sci.*, 2011, **4**, 1113.

25 M. D. Stoller, S. Park, Y. Zhu, J. An, and R. S. Ruoff, *NanoLett.*, 2008, **8**, 3498.

26 Y. Wang, Z. Shi, Y. Huang, Y. Ma, C. Wang, M. Chen, and Y. Chen, *J. Phys. Chem. C*, 2009, **113**, 13103.

27 D. Hulicova, M. Kodama, and H. Hatori, *Chem. Mater*., 2006, **18**, 2318.

28 M. M. Hantel, T. Kaspar, R. Nesper, a. Wokaun, and R. Kötz, *Electrochem. Commun.*, 2011, **13**, 90.

29 Z. J. Li, B. C. Yang, S. R. Zhang, and C. M. Zhao, *Appl. Surf. Sci.*, 2012, **258**, 3726.

30 V. Murugan, T. Muraliganth, and a. Manthiram, *Chem. Mater.*, 2009, **21**, 5004–5006.

31 L. Zhang, F. Zhang, X. Yang, G. Long, Y. Wu, T. Zhang, K. Leng, Y. Huang, Y. Ma, A. Yu, and Y. Chen, *Sci. Rep.*, 2013, **3**, 1408.

32 C. Liu, Z. Yu, D. Neff, A. Zhamu, and B. Z. Jang, *NanoLett.*, 2010, **10**, 4863.

33 H. K. Chae, D. Y. Siberio-Perez, J. Kim, Y. Go, M. Eddaoudi, A. J. Matzger, M. O'Keeffe and O. M. Yaghi, *Nature*, 2004, **427**, 523.

34 A. S. Aric`o, P. Bruce, B. Scrosati, J.-M. Tarascon and W. V. Schalkwijk, *Nat. Mater*., 2005, **4**, 366.

35 Y. G. Sun, *Nano Energy*, 2013, **2**, 811.

36 L. Nyholm, G. Nyström, A. Mihranyan, and M. Strømme, *Adv. Mater.*, 2011, **23**,3751

37 R. C. Agrawal and G. P. Pandey, *J. Phys. D. Appl. Phys.*, 2008, **41**, 223001.

38 M. Selvakumar and D. K. Bhat, *J. Appl. Polym. Sci.*, 2008, **110**, 594.

39 J. Przyluski, Z. Poitarzewski, and W. Wieczorek, *Polymer,* 1998, **39**, 4343.

40 B. G. Choi, S.-J. Chang, H.-W. Kang, C. P. Park, H. J. Kim, W. H. Hong, S. Lee, and Y. S. Huh, *Nanoscale*, 2012, **4**, 4983.

41 C. Meng, C. Liu, L. Chen, C. Hu, and S. Fan, *NanoLett.*, 2010, **10**, 4025.

42 W. Wieczorek, Z. Florjaficzyk, and J. R. Stevens*, Electrochim. Acta*, 1995, 40, 2327.

43 J. H. Chen, M. Ishigami, C. Jang, D. R. Hines, M. S. Fuhrer, and E. D. Williams, *Adv. Mater.*, 2007, **19**, 3623.

44 L. T. Le, M. H. Ervin, H. Qiu, B. E. Fuchs, and W. Y. Lee, *Electrochem. Commun.*, 2011, **13**, 355.

45 J. Ping, J. Wu, Y. Wang, and Y. Ying, *Biosens. Bioelectron.*, 2012, **34**, 70.

46 T. Lu, Y. Zhang, H. Li, L. Pan, Y. Li, and Z. Sun, *Electrochim. Acta*, 2010, **55**, 4170.

47 H. Chang, G. Wang, A. Yang, X. Tao, X. Liu, Y. Shen, and Z. Zheng, *Adv. Funct. Mater.*, 2010, **20**, 2893.

48 M. Valkiainen, S. Tuurala, M. Smolander, and O. T. Kaukoniemi. *RSC Energy and Environment Series No. 2, Innovations in Fuel Cell Technologies,* Chapter 1, printed enzymatic current sources. pp 16.

49 Y. Xu, M. G. Schwab, A. J. Strudwick, and I. Hennig, *Adv. Energy Mater.* 2013, **3**, 1035.

50 Y. N. Sudhakar and M. Selvakumar, *Electrochim. Acta*, 2012, **78**, 398.

51 W. S. Hummers, R. E. Offeman, *J. Am. Chem. Soc.*, 1958, **80**, 1339.

52 N. I. Kovtyukhova, *Chem. Mater*., 1999, **11**, 771.

53 D. R. Dreyer, S. Park, C. W. Bielawski, and R. S. Ruoff, *Chem. Soc. Rev.*, 2010, **39**, 228.

54 X. Fan, W. Peng, Y. Li, X. Li, S. Wang, G. Zhang, and F. Zhang, *Adv. Mater.*, 2008, **20**, 4490.

55 Y. N. Sudhakar and M. Selvakumar, *J. Appl. Electrochem.*, 2012, **43**, 21.

56 N. Rezlescu, and E. Rezlescu, *Phys. Status Solidi A*, 1974, **23**, 575.

57 M. Forsyth, D. R. MacFarlane, P. Meakin, M. E. Smith, and T. J. Bastow, *Electrochim. Acta*, 1995, **40**, 2131.

58 M. Selva Kumar and D. K. Bhat, *Phys. B Condens. Matter*, 2009, **404**, 1143.

59 W. Chen and L. Yan, *Nanoscale*, 2010, **2**, 559.

60 C. S. Wang, G. T. Wu, and W. Z. Li, *J. Power Sources*, 1998, **76**, 1.

61 M. Kumar, K. Singh, S. K. Dhawan, K. Tharanikkarasu, J. S. Chung, B.-S. Kong, E. J. Kim, and S. H. Hur, *Chem. Eng. J.*, 2013, **231**, 397.

62 A. C. Ferrari, *Solid State Commun.*, 2007, **143**, 47–57.

63 Y. Xu, H. Bai, G. Lu, C. Li, and G. Shi, *J. Am. Chem. Soc*. 2008, **130**, 5856.

64 A. Bagri, C. Mattevi, M. Acik, Y. J. Chabal, M. Chhowalla, and V. B. Shenoy, *Nature Chemistry*, 2010, **2,** 581.

65 http://www.intechopen.com/books/infrared-spectroscopy-materials-science-engineering-andtechnology/research-of-calcium-phosphates-using-fourier-transformation-infrared-spectroscopy.

66 M.D. Stoller, S. Park, Y. Zhu, J. An, R.S. Ruoff, NanoLett. 8 (2008) 3498.

67 K.S. Hazra, J. Rafiee, M. a Rafiee, a Mathur, S.S. Roy, J. McLauhglin, N. Koratkar, D.S. Misra, Nanotechnology 22 (2011) 025704.

68 G. Wang, L. Zhang, and J. Zhang, *Chem. Soc. Rev.*, 2012, **41**, 797.

69 A. K. Mishra and S. Ramaprabhu, *J. Phys. Chem. C*, 2011, **115**, 14006–14013.

70 X. Yang, F. Zhang, L. Zhang, T. Zhang, Y. Huang, and Y. Chen, *Adv. Funct. Mater.*, 2013, **23**, 3353.

71 Y. N. Sudhakar, M. Selvakumar, and D. K. Bhat, *Ionics.*, 2012, **19**, 277.

72 H. Yu, J. Wu, L. Fan, Y. Lin, K. Xu, Z. Tang, C. Cheng, S. Tang, J. Lin, M. Huang, and Z. Lan, *J. Power Sources*, 2012, **198**, 402.

73 F. Béguin, V. Presser, A. Balducci, and E. Frackowiak, *Adv. Mater.*, 2014, DOI: 10.1002/adma.201304137

74 C. Largeot, C. Portet, J. Chmiola, P. Taberna, Y. Gogotsi and P. Simon, *J. Am. Chem. Soc.*, 2008, **130**, 2730.

75 A. Burke, *J. Power Sources*, 2000, **91**, 37.

76 L. L. Zhang, X. Zhao, M. D. Stoller, Y. Zhu, H. Ji, S. Murali, Y. Wu, S. Perales, B. Clevenger, and R. S. Ruoff, *NanoLett.*, 2012, **12**, 1806–12.

77 Z. Li, J. Wang, S. Liu, X. Liu, and S. Yang, *J. Power Sources*, 2011, **196**, 8160–8165.

78 B. Zhao, P. Liu, Y. Jiang, D. Pan, H. Tao, J. Song, T. Fang, and W. Xu, *J. Power Sources*, 2012, **198**, 423–427.

79 Y. Shao, J. Wang, M. Engelhard, C. Wang, and Y. Lin, *J. Mater. Chem.*, 2010, **20**, 743.

80 K. Zhang, L. Mao, L. L. Zhang, H. S. On Chan, X. S. Zhao, and J. Wu, *J. Mater. Chem.*, 2011, **21**, 7302.

81 Y. Chen, X. Zhang, D. Zhang, P. Yu, and Y. Ma, *Carbon*, 2011, **49**, 573–580.

82 A. Chidembo, S. H. Aboutalebi, K. Konstantinov, M. Salari, B. Winton, S. A. Yamini, I. P. Nevirkovets, and H. K. Liu, *Energy Environ. Sci.*, 2012, **5**, 5236.

83 Y. Zhu, S. Murali, M. D. Stoller, A. Velamakanni, R. D. Piner, and R. S. Ruoff, *Carbon*, 2010, **48**, 2118–2122.

84 M. Yamagata, S. Ikebe, K. Soeda, and M. Ishikawa, *RSC Adv.*, 2013, **3**, 1037.

85 C. Xiang, M. Li, M. Zhi, A. Manivannan, and N. Wu, *J. Mater. Chem.*, 2012, **22**, 19161.

86 K. Karthikeyan, D. Kalpana, S. Amaresh, and Y. S. Lee, *RSC Adv.*, 2012, **2**, 12322.

87 J. Wang, Z. Gao, Z. Li, B. Wang, Y. Yan, Q. Liu, T. Mann, M. Zhang, and Z. Jiang, *J. Solid State Chem.*, 2011, **184**, 1421–1427.

88 K. Karthikeyan, S. Amaresh, V. Aravindan, and Y. S. Lee, *J. Mater. Chem. A*, 2013, **1**, 4105.

89 J. Zhang, G. Shen, W. Wang, X. Zhou, and S. Guo, *J. Mater. Chem.*, 2010, **20**, 10824.

Figure captions

Fig. 1 (a) Variations of conductivities of SPEs at different temperature, (b) Nyquist impedance plots of the SPE at different temperatures

Fig. 2 Plots of dielectric studies versus frequency at different temperatures (a) dielectric constant, (b) dielectric loss, (c) real part of electric modulus, and (d) imaginary part of electric modulus of 1M H_3PO_4 doped GPE.

Fig. 3 (a) XRD pattern of battery graphite, rGO and rGO+binder, (b) Raman spectrum of GO and rGO, (c) FTIR spectra of graphite, GO and rGO, and (d) FTIR spectra of pure PVP, PVP+H_3PO_4 and PVP+rGO

Fig. 4 (a and b) C1s and O1s XPS spectra of GO, (c and d) C1s and O1s XPS spectra of rGO

Fig. 5 (a) rGO powder, (b and c) screen printed rGO+PVP binder top and cross section view

Fig. 6 (a) TEM image of rGO powder, (b) SAED of rGO sheets.

Fig. 7 (a) CVs of supercapacitor at different scan rates, (b) AC impedance plot of supercapacitor, (c) Plots of normalized reactive power $|Q|/|S|\%$ and active power $|P|/|S|\%$ versus frequency (Hz), (d) GCD plots at different current densities, and (e) Variation of specific capacitance of the supercapacitor during long-term cycling.

Scheme 1 Screen printing of rGO+binder and SPE on PET and fabrication of supercapacitor with possible mechanism of ions transportation

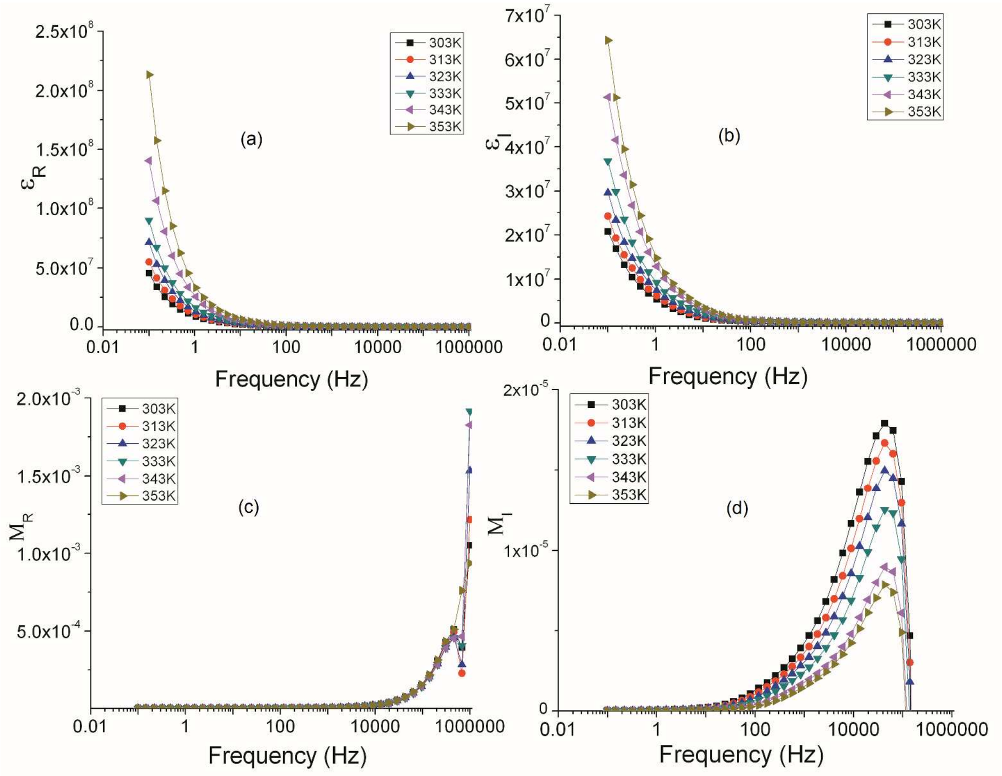

Fig. 2 Plots of dielectric studies versus frequency at different temperatures (a) dielectric constant, (b) dielectric loss, (c) real part of electric modulus, and (d) imaginary part of electric modulus of 1M H3PO4 doped GPE.
297x229mm (300 x 300 DPI)

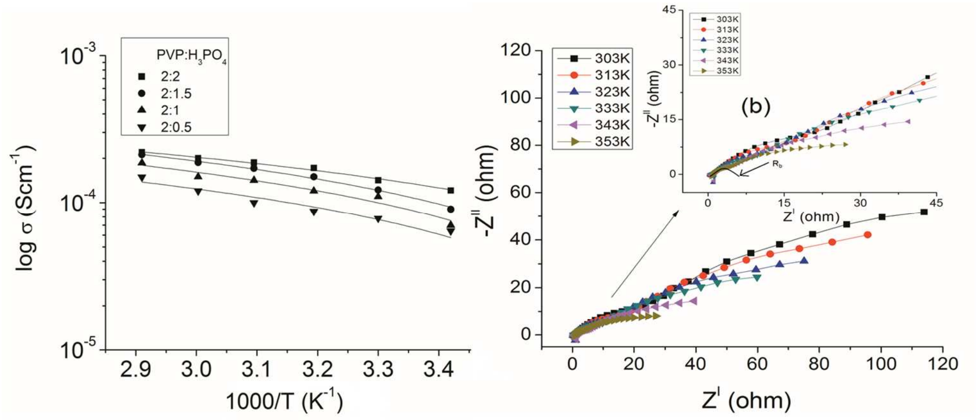

Fig. 1 (a) Variations of conductivities of SPEsat different temperature, (b) Nyquist impedance plots of the SPE at different temperatures
440x186mm (96 x 96 DPI)

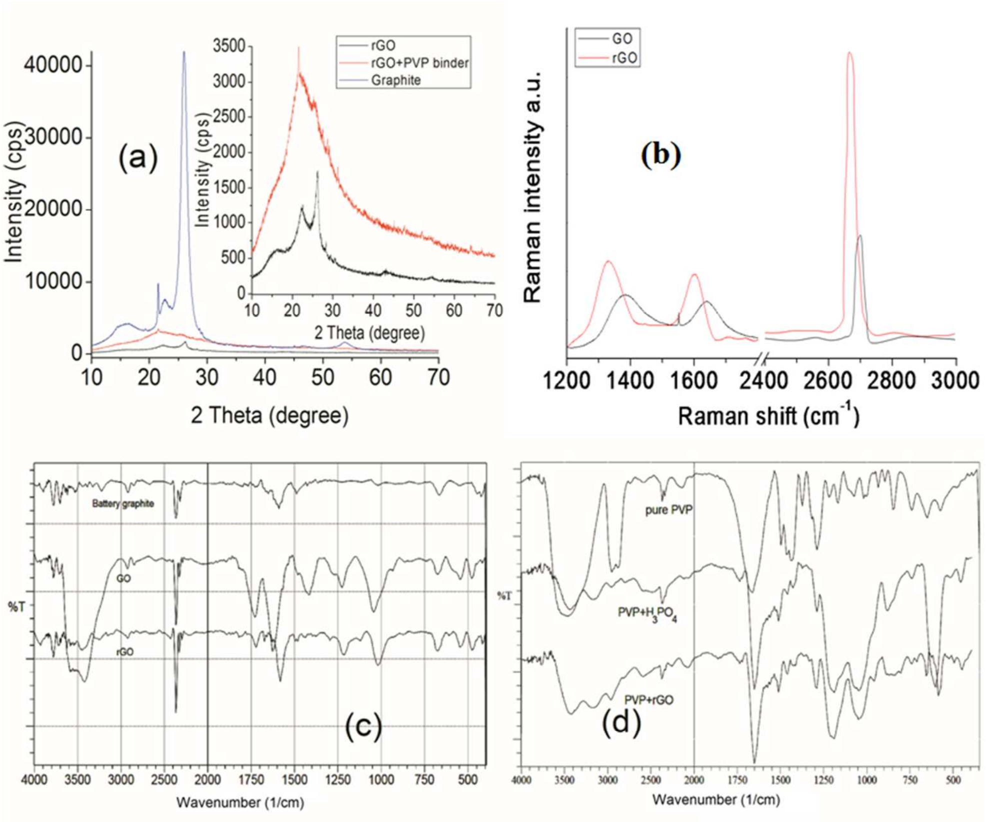

Fig. 3 (a) XRD pattern of battery graphite, rGO and rGO+binder, (b) Raman spectrum of GO and rGO, (c) FTIR spectra of graphite, GO and rGO, and (d) FTIR spectra of pure PVP, PVP+H3PO4 and PVP+rGO
229x191mm (96 x 96 DPI)

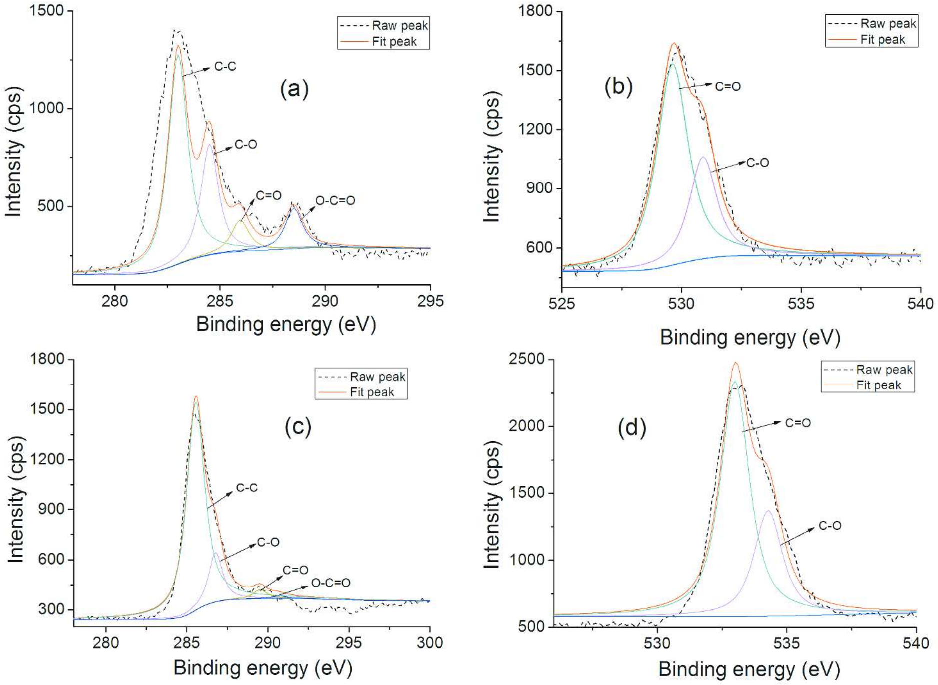

Fig. 4 (a and b) C1s and O1s XPS spectra of GO, (c and d) C1s and O1s XPS spectra of rGO
287x202mm (300 x 300 DPI)

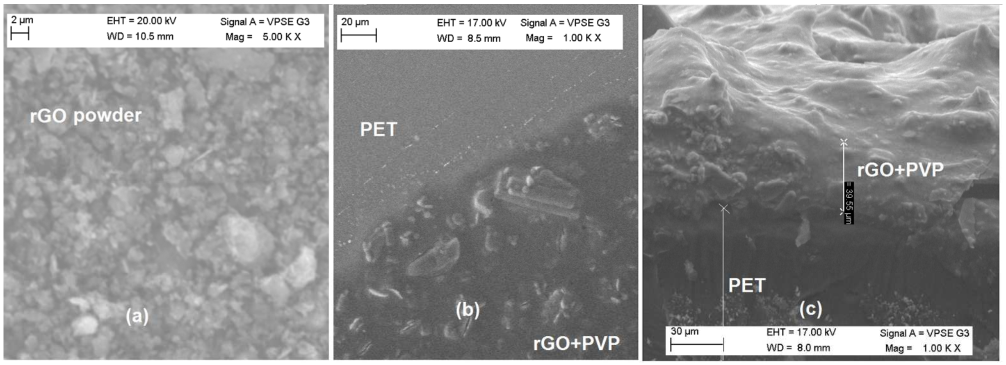

Fig. 5 (a) rGO powder, (b and c) screen printed rGO+PVP binder top and cross section view
512x183mm (96 x 96 DPI)

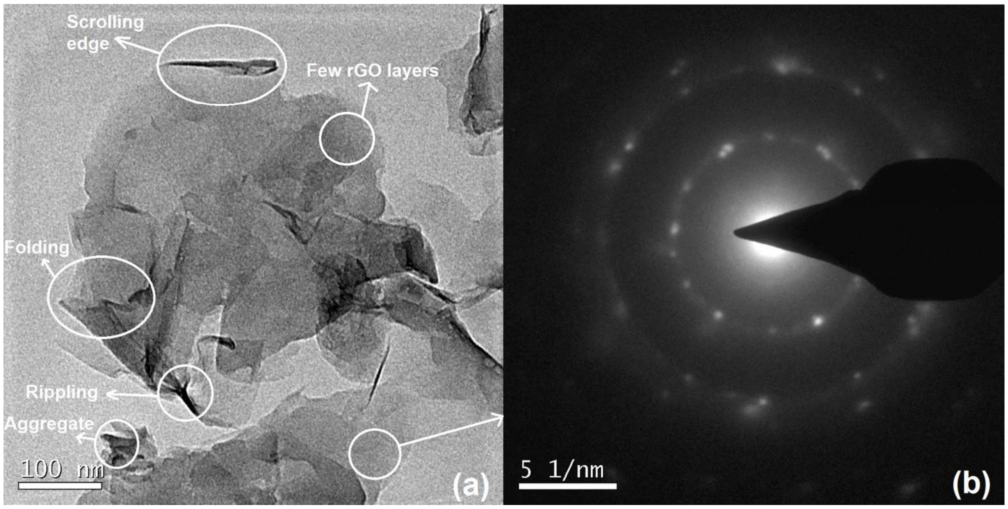

Fig. 6 (a) TEM image of rGO powder, (b) SAED of rGO sheets
541x270mm (96 x 96 DPI)

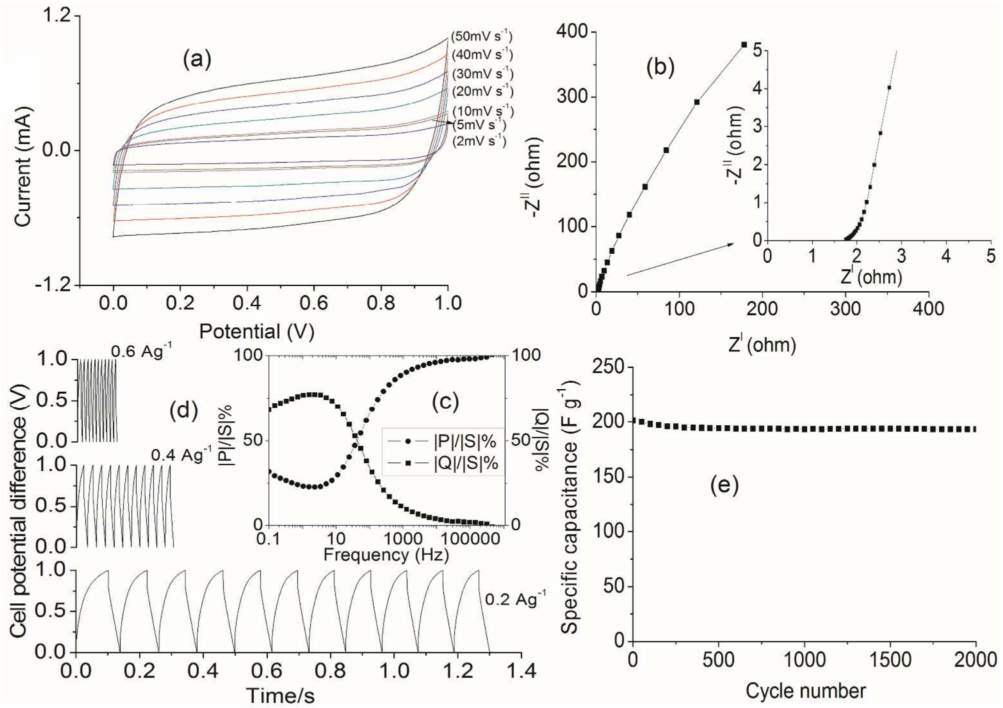

Fig. 7 (a) CVs of supercapacitor at different scan rates, (b) AC impedance plot of supercapacitor, (c) Plots of normalized reactive power |Q|/|S|% and active power |P|/|S|% versus frequency (Hz), (d) GCD plots at different current densities, and (e) Variation of specific capacitance of the supercapacitor during long-term cycling.
287x202mm (300 x 300 DPI)

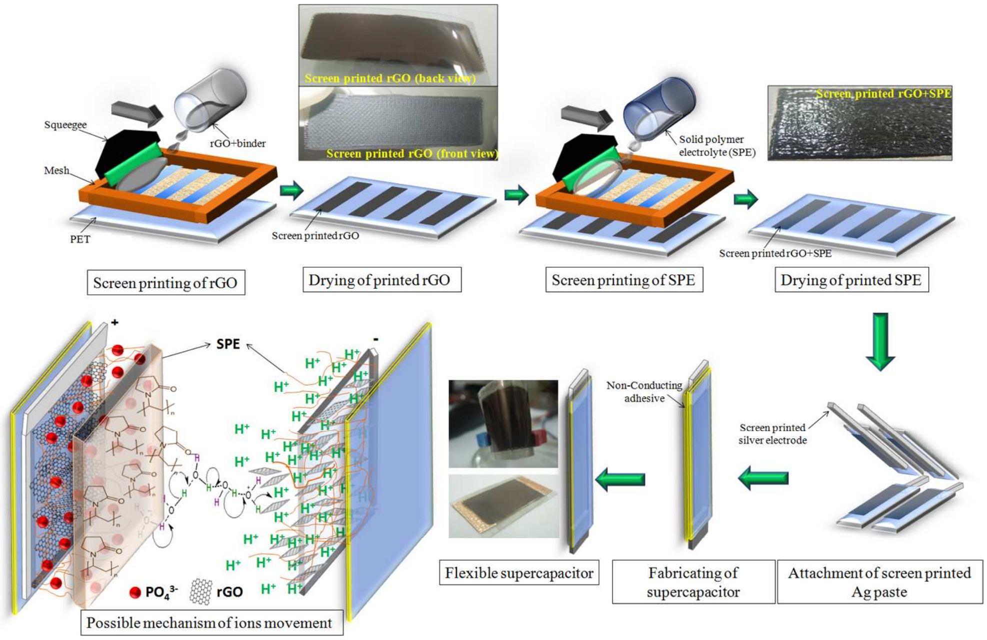

Screen printing of rGO+binder and SPE on PET and fabrication of supercapacitor with possible mechanism of ions transportation
450x288mm (96 x 96 DPI)

Table 1. Comparison of rGO derived from different methods and their specific capacitance

Electrode material and electrolyte	Reducing method	Specific capacitance	Ref.
Porous Activated rGO, $TEABF_4$/AN	KOH+800 °C	GCD: 120 F g^{-1} at 10 A g^{-1}	76
rGO+MnO_2, 1M Na_2SO_4	hydrothermally	CV: 211.5 F g^{-1} at 2 mV s^{-1}	77
rGO sheets, 6M KOH	thermal	GCD: 260.5 F g^{-1} at 0.4 A g^{-1}	78
rGO, 0.1M Na_2SO_4	electrochemical	CV: 164.8 F g^{-1} at 20 mV s^{-1} GCD: 150.4 F g^{-1} at 5 A g^{-1}	79
rGO, 2M H_2SO_4	surfactants	GCD: 194 F g^{-1} at 1 A g^{-1}	80
rGO, KOH	chemically using hydrazine	205 F g^{-1} at 0.1 A g^{-1}	26
rGO, 1M H_2SO_4	hydrobromic acid, 110 °C	348 F g^{-1} at 0.2 A g^{-1}	81
rGO+metal oxide	Spray pyrolysis	CV: 687 F g^{-1} at 5 mV s^{-1}	82
rGO	Ionic liquid assisted microwave reduction	135 F g^{-1} at 2 A g^{-1}	15
Exfoliated rGO	microwave	191 F g^{-1} at 150 mA g^{-1}	83
rGO/PVP binder, PVP+H_3PO_4	$CaCO_3$ and microwave	CV:201 F g^{-1} at 2 mV s^{-1} GCD: 208 F g^{-1} at 0.2 A g^{-1}	Present work

Table 2. Comparison of power density and energy density of various electrode materials.

Power density (W kg^{-1})	Energy density (Wh kg^{-1})	Electrode material and electrolyte	Ref.
9838 at 8 A g^{-1}	90 at 0.5 A g^{-1}	Graphene, $EMIMBF_4$	32
6.8k at 10 A g^{-1}	19.7 at 0.5 A g^{-1}	rGO+RuO_2/rGO, PVA+ H_2SO_4	40
246k at 8 A g^{-1}	58 at 2 A g^{-1}	rGO,EMIM.NTf_2	15
32k	15	Activated carbon, $TEMABF_3$	84
170	20.1	rGO+TiO_2	85
200	11	rGO+Fe_3O_4	86
500	26	rGO, $TEABF_3$	76
8.1k		rGO+ZnO	87
0.22k	30	MgO+ Carbon Nanotude, 1M $LiPF_6$	88
2k at 0.2 A g^{-1}	11 at 0.2 A g^{-1}	rGO/PVP binder, PVP+H_3PO_4	Present work